C−C versus C−H Bond Activation of Alkynes by Early Second-Row Transition Metal Atoms

Ryan Z. Hinrichs, Jonathan J. Schroden, and H. Floyd Davis*

Department of Chemistry and Chemical Biology, Cornell University, Ithaca, New York 14853

Received: January 4, 2008

The reactions of Y (a^2D), Zr (a^3F), Nb (a^6D), Mo (a^7S), and electronically excited-state Mo* (a^5S) with propyne (methylacetylene) and 2-butyne (1,2-dimethylacetylene) were investigated using crossed molecular beams. For all of the metals studied, reactions with propyne led to H_2 elimination, forming MC_3H_2. For Y + propyne, C−C bond cleavage forming YCCH + CH_3 also was observed, with an energetic threshold in good agreement with an earlier determination of D_0(Y−CCH). For Y + 2-butyne, three reactive channels were observed: $YC_4H_4 + H_2$, $YC_3H_3 + CH_3$, and $YC_3H_2 + CH_4$. The C−C bond cleavage products accounted for 21 and 27% of the total products at $E_{coll} = 69$ and 116 kJ/mol, respectively. For Zr and Nb reactions with 2-butyne, competition between H_2 and CH_4 elimination was observed, with C−C bond cleavage accounting for 12 and 4% of the total product signal at $E_{coll} = 71$ kJ/mol, respectively. For reactions of Mo and Mo* with 2-butyne, only H_2 elimination was observed. The similarity between reactions involving two isomeric species, propyne and allene, suggests that H atom migration is facile in these systems.

Introduction

The oxidative addition of covalent bonds to transition metal centers, M + R−R′ → R−M−R′, plays a significant role in many catalytic and bond-activation processes.[1,2] For reactions with hydrocarbons, two oxidative addition processes may compete: activation of a carbon−hydrogen (C−H) bond or activation of a carbon−carbon (C−C) bond.[1−10] For reactions of transition metal cations with small molecules in the gas phase, the competition between these processes has been studied quite extensively.[6,7] However, for neutral transition metal atoms, which are in general much less reactive with hydrocarbon molecules,[7] C−C bond activation is relatively uncommon.[8−10]

A number of complementary approaches have been taken in theoretical studies of transition metal−hydrocarbon reactions. In one approach, detailed theoretical calculations were carried out for reactions of one or a small number of realistic transition metal systems containing ligands.[11] An alternative approach involved studying trends in reactivity of a large number of closely related model systems.[3,4,12] For example, the reactions of bare neutral transition metal atoms with simple hydrocarbons such as CH_4 were studied theoretically for all three rows of the periodic table.[12] The activation of C−H bonds by transition metal atoms involves the donation of electron density from the C−H σ-bonding orbital into metal acceptor orbitals of σ-symmetry, with concurrent back-donation from occupied metal d orbitals into the σ*-antibonding orbital. Metal s^0d^n electronic configurations were found to be optimal for reducing reactant repulsion upon approach to the transition state (TS), while the formation of two covalent bonds in the C−M−H intermediate was most favorable for low-spin s^1d^{n-1} electronic configurations.[3,7] For neutral second-row transition metal atoms, the ground electronic states typically have s^2d^{n-2} configurations.[7,13] Therefore, barriers for C−H and C−C insertion result from the avoided crossing between diabatic curves correlating to the ground-state atom and the atomic state(s) leading to the reaction.[4,7]

It has been noted previously that although the C−H bond energies increase going from ethane (432 kJ/mol) to ethene (459 kJ/mol) to ethyne (549 kJ/mol),[14] the potential energy barrier heights for C−H insertion by second-row transition metal atoms actually decrease.[3] Since insertion requires favorable orbital overlap between the metal and the C−H σ-bond at the transition state, steric considerations likely play an important role in determining barrier heights.[3] It also has been known for many years that alkenes and alkynes can form strongly bound (120−250 kJ/mol) π-association complexes between the metal and the C−C double and triple bonds.[3,4] Alkanes, on the other hand, can only form weakly bound (<8 kJ/mol) σ-complexes prior to C−H insertion.[1,12] Although the ability of alkenes and alkynes to form complexes has been thought to play an important role in reducing barriers for reaction,[3,4,15] in some cases, evidence has been presented that complex formation does not necessarily precede C−H insertion.[16]

We previously have studied the reactions of early second-row transition metal atoms with various hydrocarbons. For saturated hydrocarbons (methane, ethane, and propane), only C−H bond activation is observed, yielding dehydrogenation products (e.g., $MCH_2 + H_2$, $MC_2H_4 + H_2$, etc.), or in some cases, formation of the metal dihydride, HMH.[17−19] These results are consistent with ab initio calculations that find C−C bond-activation barriers to be larger than C−H bond-activation barriers by 40−80 kJ/mol for neutral metal atom reactions with alkanes.[3,4] Reactions of ground-state Y, Zr, Nb, and Mo* with propene also yield dehydrogenation products.[10,20] For Y + propene, C−C bond activation was also observed, producing $YCH_2 + C_2H_4$.[10] However, the reaction does not involve insertion of Y into the sp^3−sp^2 C−C bond but instead involves π-complex formation followed by β-C−H bond activation, with subsequent H migration to form a four-membered ring intermediate (metallocyclobutane), which then decays to give YCH_2

* Author to whom correspondence should be addressed. E-mail: hfd1@cornell.edu.

10.1021/jp800077m CCC: $40.75
Published on Web 03/19/2008

$+ C_2H_4$ products.[10] A similar mechanism was proposed for YCH_2 formation from reactions of Y with four butene isomers.[8]

In reactions of $Y + C_2H_2$, C−H activation leading to the formation of $YC_2 + H_2$ was found to be dominant.[21] As in the studies of reactions involving alkenes,[9] strong nonreactive wide-angle scattering of metal atoms was observed, demonstrating that a substantial fraction of initially formed π-complexes decayed back to reactants. At sufficiently high collision energies, the formation of YCCH + H also was observed. From the observed threshold behavior for this reaction, we concluded that $D_o(Y-CCH) = 461.1 \pm 8.4$ kJ/mol.[21]

In this study, we observed a number of competing pathways for reactions of second-row transition metal atoms with propyne and 2-butyne. For ground-state Y atoms, the following reactions were observed:[22−28]

$$Y + CH_3CCH \rightarrow YC_2H + CH_3 \quad \Delta E \approx +60 \text{ kJ/mol}$$

$$\rightarrow YC_3H_2 + H_2 \quad \Delta E \approx -130 \text{ kJ/mol}$$

$$Y + CH_3CCCH_3 \rightarrow YC_3H_3 + CH_3 \quad \Delta E \approx +70 \text{ kJ/mol}$$

$$\rightarrow Y(C_2H_2)_2 + H_2 \quad \Delta E \approx -100 \text{ kJ/mol}$$

$$\rightarrow YC_3H_2 + CH_4 \quad \Delta E \approx -140 \text{ kJ/mol}$$

The goal of the present study was to explore the competition between C−H and C−C activation in reactions of alkynes containing three or four carbon atoms with Y, Nb, Zr, and Mo.

Experimental Procedures

The reactions with propyne and 2-butyne were investigated using a rotatable source crossed molecular beams apparatus.[29] Neutral metal atoms were produced by laser vaporization[30] and entrained in a supersonic expansion of an inert carrier gas (He or Ne). The resulting atomic electronic-state populations were characterized by laser induced fluorescence (LIF) excitation spectroscopy. For Y, Zr,[31] and Mo,[17] only the ground electronic states (a^2D, a^3F, and a^7S, respectively) were observed. For Nb, small populations of excited a^4F and a^4P states were observed in addition to the ground a^6D state.[31] From the LIF signal intensities, these populations were estimated to be several percent of the ground-state populations. Reactions of excited, metastable Mo* (a^5S) were studied by pumping the $z^5P_3^0 \leftarrow a^7S_3$ transition near 345 nm using a frequency-doubled dye laser.[17] The Mo* (a^5S) state resulted from decay of the $z^5P_3^0$ state, as described previously.[17]

The propyne molecular beam was generated by expanding a 10% gaseous mixture in He through a pulsed valve at a total pressure of 900 Torr.[32] A molecular beam of 2-butyne was produced by bubbling He through a neat 2-butyne sample held at −27 °C, resulting in a ~10% mixture at a total pressure of 900 Torr. Scattered products were detected 24.1 cm away from the interaction region using 157 nm photoionization followed by quadrupole mass spectrometric identification. Nonreactively scattered metal atoms were detected state-specifically using 1 + 1 resonance enhanced multiphoton ionization (REMPI). Time-of-flight (TOF) spectra for all scattered species were recorded by scanning the delay of the ionization laser with respect to time zero of the reaction. Product angular distributions were obtained by rotating the molecular beams with respect to the fixed detector. A forward convolution fitting program was used to extract the angular, $T(\theta)$, and translational energy release, $P(E)$, distributions in the center-of-mass (CM) reference frame. Both the atomic and the molecular beams undoubtedly contained small populations of van der Waals clusters. However, since the product angular distributions in all cases peaked near the CM angle, the signals reported in this paper result from reactions of monomeric atoms and molecules.

Photodepletion studies were performed for Nb to investigate the role of the ground a^6D electronic state in product formation.[31] Frequency-doubled dye laser radiation (6 mJ) was introduced upstream of the interaction region to deplete the Nb beam by 1 + 1 REMPI of ground-state atoms. To maintain alignment while the molecular source was rotated, the depletion laser was aligned along the axis of rotation and periscoped 1 cm upstream of the reaction zone using a 0.75 in. thick window tilted at 45° and mounted to the rotatable source. Because the detector lenses were held at +100 V, metal ions or the ionic products of their reactions were unable to enter the detector. The $z^4S_{3/2}^0 \leftarrow a^6D_{3/2}$ and $y^4P_{5/2}^0 \leftarrow a^6D_{5/2}$ transitions were simultaneously pumped near 358 nm.[13] The similarity between the fractional depletion of the Nb ground-state reactant beam to the depletion of the product signal indicated that the products resulted primarily from reactions of ground-state Nb a^6D atoms.

Results

M + Propyne. *Nonreactive Scattering.* Nonreactive scattering of M from propyne was recorded for lab angles $\Theta = 5-50°$, where $\Theta = 0°$ corresponds to the M atomic beam. Figure 1 shows representative TOF spectra recorded using REMPI for the ground states of Y through Mo at a collision energy (E_{coll}) of 99 kJ/mol. For Mo (a^7S), the solid lines in Figure 1 were generated using a forward peaking CM angular distribution, $T(\theta)$ (Figure 2a). The Mo (a^7S) data were simulated using two weighted $T(\theta)$ distributions (dotted and dashed lines in Figure 2a) associated with two separate $P(E)$ distributions. For Y, Zr, and Nb, a slow peak (~190 μs) became more significant at wider angles, and it was necessary to use a symmetric, forward−backward peaking $T(\theta)$ as shown in Figure 2b in addition to a forward peaking $T(\theta)$ similar in shape to that in Figure 2a. Each $T(\theta)$ distribution was associated with a separate $P(E)$ distribution. The solid-line fits shown for Y, Zr, and Nb in Figure 1 are the sum of the contributions from the forward peaking $T(\theta)$ (dotted lines) and from the forward−backward peaking $T(\theta)$ (dashed−dotted lines). Figure 3 shows the TOF spectra for Mo* nonreactive scattering, obtained with the pump laser turned on. As shown in the lower part of Figure 3, the forward scattered component decreases, and the symmetric component increases when the laser is turned on. The contribution from the symmetric component decreases in the order Y(26%) > Mo*(20%) > Nb-(17%) > Zr(8%) > Mo(0%).

H_2 Elimination. The reaction M + propyne $\rightarrow MC_3H_2 + H_2$ was observed for all ground electronic-state atoms studied and for Mo* (a^5S). Figure 4 shows laboratory angular distributions for MC_3H_2 products ($E_{coll} \approx 50$ kJ/mol) for each metal. Photodepletion of Nb (a^6D) from the atomic beam was correlated to depletion of the NbC_3H_2 product signal at several lab angles, unambiguously identifying the reaction as occurring primarily from ground-state Nb atoms.

The H_2 elimination data were simulated using the $P(E)$ distributions included in Figure 5 (top panel) with a nearly isotropic $T(\theta)$ distribution that was symmetric with respect to $\theta = 90°$. The translational energy released to products was largest for the reaction with Y and identical for reactions with Zr, Nb, and Mo*. Comparing Mo (a^7S) to Mo* (a^5S) indicated that a slightly larger amount of translational energy was deposited in products from Mo* reactions. As shown in Figure 5 (bottom panel), the $P(E)$ values were divided by the total

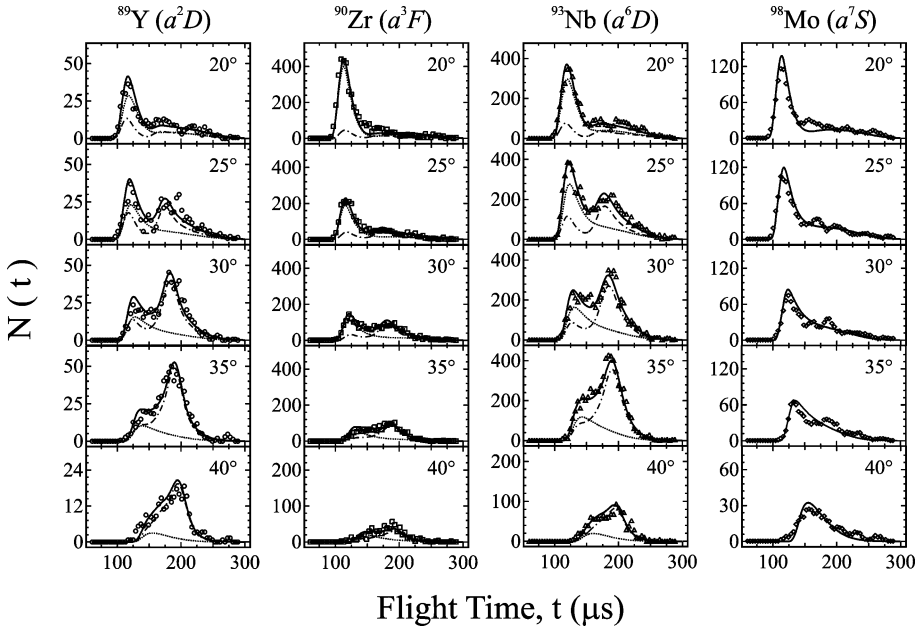

Figure 1. Nonreactive TOF spectra of ground-state metal reactants at $E_{coll} \approx 99$ kJ/mol for the M + propyne reaction (open symbols) at indicated lab angles. For Y, Zr, and Nb, solid-line fits were the sum of two processes: forward scattering (dotted lines) and decay of a long-lived complex (dashed−dotted lines). For Mo (a^7S), only forward scattering was observed.

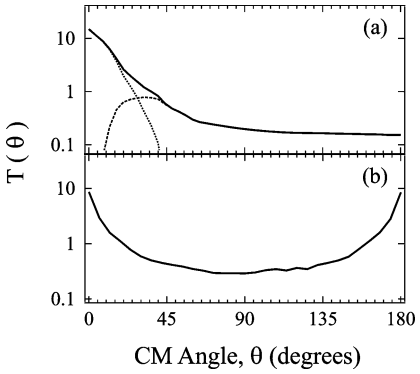

Figure 2. (a) CM angular distribution used to generate fits for Mo + propyne nonreactive scattering TOF spectra (Figure 1). See text for details. (b) CM angular distribution used to generate dashed−dotted line contributions to solid-line fits for Y, Zr, and Nb + propyne nonreactive scattering TOF spectra (Figure 1). Dotted line contributions to the fits in Figure 1 were generated using a CM angular distribution similar in shape to that in panel a.

amount of available energy. We observed a greater translational energy release for Y as compared to Zr and Nb (e.g., $\langle f_T(Y) \rangle = 0.29$ as compared to $\langle f_T(Zr) \rangle = 0.25$).

CH_3 Elimination. The reaction M + propyne → MC_2H + CH_3 was only observed for Y. The TOF spectra for YC_2H products obtained at $E_{coll} = 99$ kJ/mol are shown in Figure 6 and have been corrected for a minor contribution from fragmentation of YC_3H_2 (0.7% of the *m*/*e* 127 signal). The solid-line fits were generated using the CM distributions included in Figure 7. The average CM translational energy release was 22 kJ/mol, and the $T(\theta)$ distributions peaked in the forward and backward directions with $T(0°)/T(90°) = 5.5$. Assuming equal 157 nm photoionization cross-sections for YC_2H and YC_3H_2,[9,10] the product branching ratio, $\phi_{YC_2H}/\phi_{YC_3H_2}$, was 0.11:1.00. The lab angular distributions for these two competing product channels for Y + propyne are shown in Figure 8a.

Competition between CH_3 and H_2 elimination was monitored as a function of E_{coll} (Figure 8). At the lowest E_{coll} studies (50 and 54 kJ/mol), a weak signal recorded at *m*/*e* 114 was identical in form to the *m*/*e* 127 signal, at 0.7% of the intensity. We

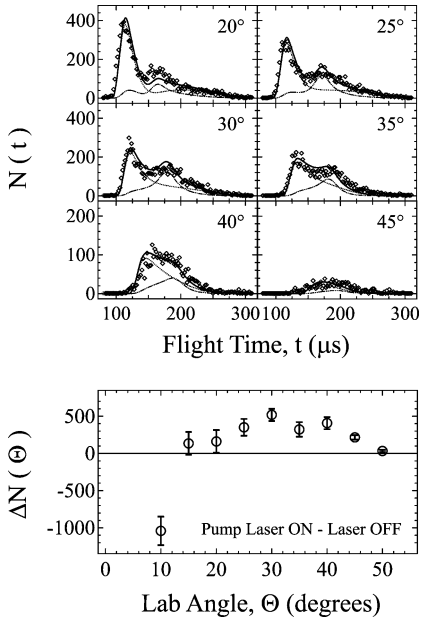

Figure 3. Top: nonreactive TOF spectra for Mo + propyne with pump laser on, for example, Mo (a^7S_3) and Mo* (a^5S_2) nonreactive scattering. Bottom: lab angular distribution for pump laser on minus laser off.

concluded that the *m*/*e* 114 signal at this E_{coll} value was due to fragmentation of YC_3H_2. The real YC_2H signal was observed at $E_{coll} \geq 63$ kJ/mol. While simulation of all experimental data required convolution over the E_{coll} distribution (Figure 9, top panel), YC_2H data obtained near this threshold required a step-function cutoff to accurately fit the width and arrival times for the YC_2H TOF spectra.[21] Thus, only collisions at energies above the threshold were able to form products. At the lowest E_{coll} where CH_3 elimination was observed, a cutoff value of 63 ± 4 kJ/mol was used. Further experiments near this threshold collision energy found that as E_{coll} increased, the best-fit energy threshold shifted to higher energies. For example, at $E_{coll} = 79$ kJ/mol, the best-fit cutoff was 67 ± 4 kJ/mol. This behavior is similar to that observed in the Y + C_2H_2 reaction.[21] The maximum translational energy released for YC_2H at each E_{coll}

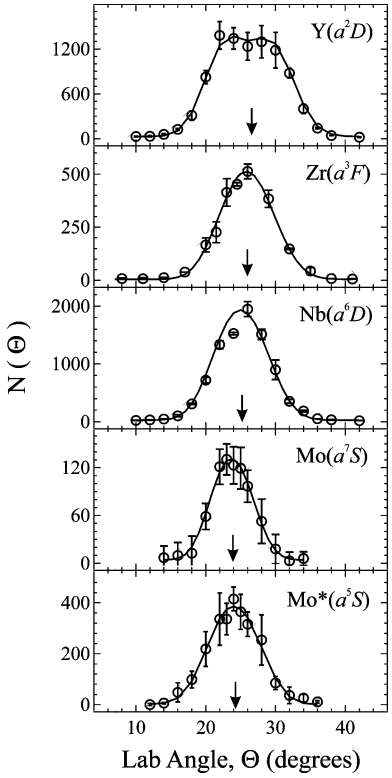

Figure 4. Lab angular distributions for MC_3H_2 products (H_2 elimination) from the M + propyne reaction recorded at E_{coll} = 50 kJ/mol (open symbols). Solid-line fits generated using translational energy distributions shown in Figure 5. Distributions have been scaled to the same data acquisition time. Arrows denote center of mass angle for each system.

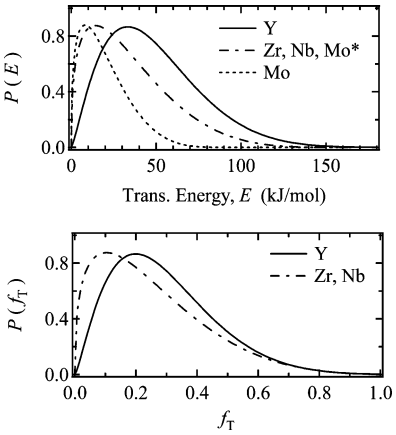

Figure 5. Translational energy release distributions, $P(E)$ and $P(f_T)$, for H_2 elimination from M + propyne used to generate solid-line fits included in Figure 4.

value was consistent with this threshold (see, i.e., Figure 7). A plot of the product branching ratio as a function of E_{coll} is shown in Figure 9 (lower panel).

Y + Allene. The reaction of Y with allene (CH_2═C═CH_2), a structural isomer of propyne with nearly the same enthalpy of formation, was studied at a collision energy E_{coll} = 84 kJ/mol. The formation of YC_2H + CH_3, as well as YC_3H_2 + H_2, was observed. The branching ratio and translational energy disposal were found to be very similar to Y + propyne. The nonreactive scattering of Y + CH_2═C═CH_2 was also studied. As in the case of Y + propyne, strong wide-angle scattering of Y was observed, indicating that a large fraction of collisions formed π-association complexes.

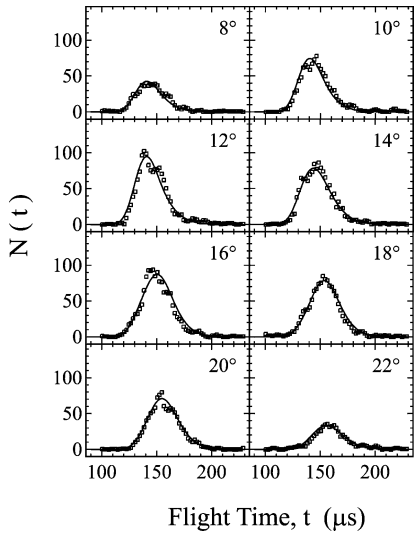

Figure 6. Sample TOF spectra for YC_2H products from the Y + propyne reaction at indicated lab angles recorded at E_{coll} = 99 kJ/mol (open squares). Solid-line fits were generated using the CM distributions shown in Figure 7.

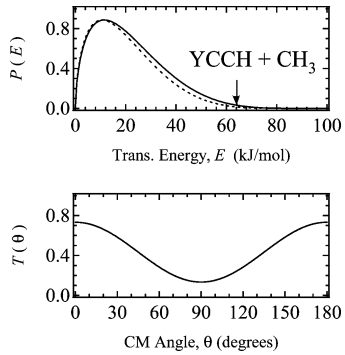

Figure 7. CM distributions for Y + propyne → YC_2H + CH_3 used to generate the fits shown in Figure 6. Dotted line in $P(E)$ corresponds to the range of distributions that gave acceptable fits (analogous to error bars). Arrow in $P(E)$ indicates the thermodynamic threshold for YC_2H production.

M + 2-Butyne. *Y (a^2D) + 2-Butyne.* The reaction of Y with 2-butyne was investigated at E_{coll} = 69 and 116 kJ/mol. Three products were detected: YC_4H_4 (*m*/*e* 141), YC_3H_3 (*m*/*e* 128), and YC_3H_2 (*m*/*e* 127). Lab angular distributions for competing channels recorded under identical conditions at E_{coll} = 69 kJ/mol are shown in Figure 10; those at the higher E_{coll} values looked similar and are not shown. The optimized CM translational energy release distribution, $P(E)$, and CM angular distribution, $T(\theta)$, for each product channel are shown in Figure 11. The $T(\theta)$ distributions were symmetric with respect to θ = 90° and peaked in the forward and backward directions. Using the binding energy for YC_3H_2 derived for the Y + propyne reaction, the average fraction of total available energy released as translational energy for YC_3H_2 + CH_4 was $\langle f_T(YC_3H_2)\rangle$ = 0.32.

The lab angular distributions depicted in Figure 10 represent the same number of laser shots for each product channel. Methane elimination comprised 19% of the product signal at E_{coll} = 69 kJ/mol (Table 1).[9] The relative amount of CH_3 elimination increased from 2 to 15% at the higher collision energy.

Zr (a^3F) + 2-Butyne. Two channels were observed: ZrC_4H_4 + H_2 and ZrC_3H_2 + CH_4. Laboratory angular distributions recorded at *m*/*e* 142 ($^{90}ZrC_4H_4^+$) and *m*/*e* 128 ($^{90}ZrC_3H_2^+$) are shown in Figure 12. The product branching ratio, $\phi_{ZrC_3H_2}/\phi_{ZrC_4H_4}$, was 0.14:1.00 (Table 1). While the lab angular distribution for

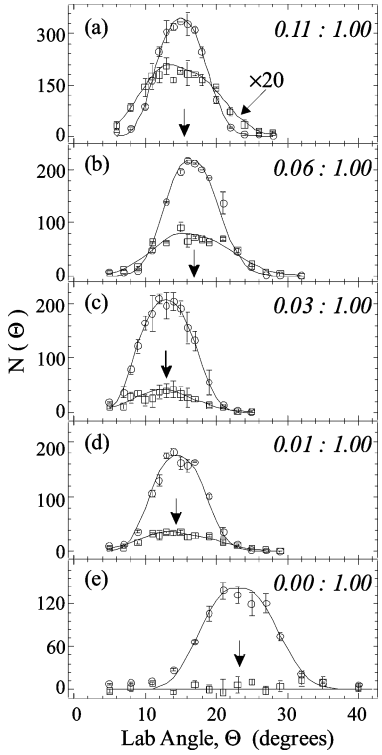

Figure 8. Lab angular distributions for YC_3H_2 (circles) and YC_2H (squares) products from the Y + propyne reaction recorded at E_{coll} = (a) 99, (b) 80, (c) 75, (d) 69, and (e) 56 kJ/mol. Product branching ratio, $\phi_{YC_2H}/\phi_{YC_3H_2}$, included in the upper right corner of each panel. Distributions for YC_2H products were multiplied by a factor of 20 at each collision energy for presentation. Arrows denote center of mass angle for each system.

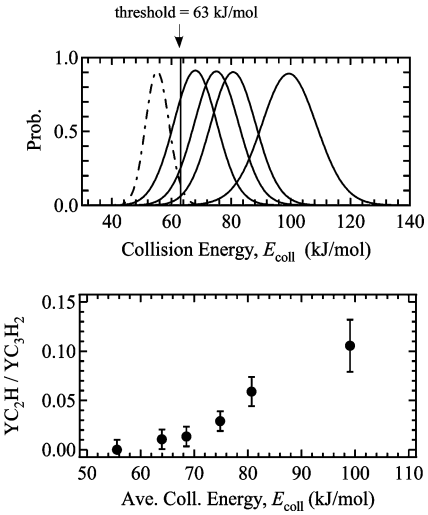

Figure 9. Top: collision energy distributions a−e associated with Y + propyne data shown in Figure 8, with measured threshold for CH_3 elimination. Bottom: product branching ratio, $\phi_{YC_2H}/\phi_{YC_3H_2}$, vs E_{coll}.

H_2 elimination appears qualitatively similar to that for YC_4H_4, the CH_4 elimination angular distribution peaked near Θ_{CM}, in contrast to the broad distribution observed for YC_3H_2 (Figure 10). In simulating the data for this product channel, the $T(\theta)$ distribution was similar to that for Y, but the $P(E)$ distribution was distinct. Using the values for MC_3H_2 binding energies from the H_2 elimination channels for propyne, the $P(E)$ values for CH_4 elimination from 2-butyne were converted to $P(f_T)$ (Figure 13). The average value of energy released as translational energy, $\langle f_T(ZrC_3H_2)\rangle$, was 0.23.

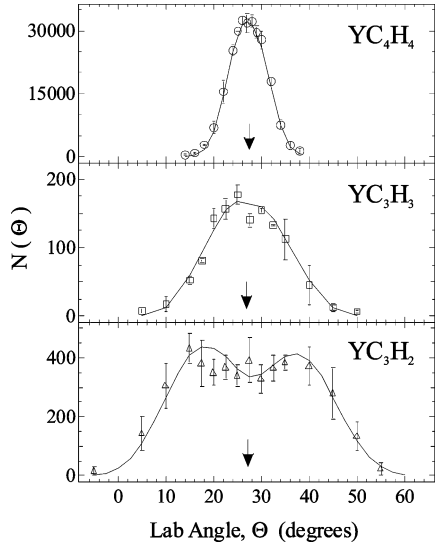

Figure 10. Lab angular distributions for YC_4H_4 (circles), YC_3H_3 (squares), and YC_3H_2 (triangles) products from the Y + 2-butyne reaction recorded at E_{coll} = 69 kJ/mol. Distributions have been normalized to the same number of laser shots. Solid-line fits generated using CM distributions shown in Figure 11. Arrows denote center of mass angle for each system.

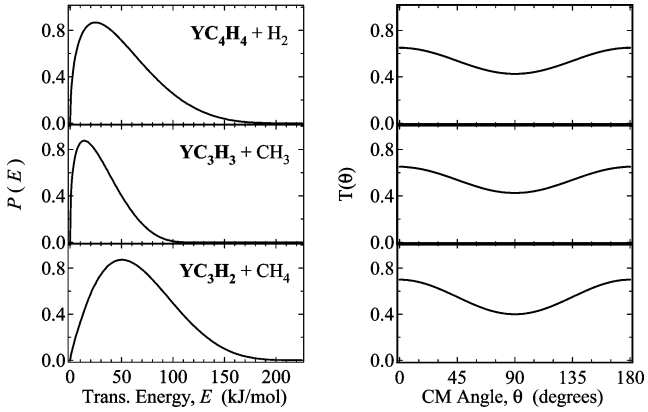

Figure 11. CM distributions for competing product channels used to generate fits to the data resulting from collisions of Y + 2-butyne at E_{coll} = 69 kJ/mol shown in Figure 10.

TABLE 1: M + 2-Butyne Product Branching Ratios

metal	E_{coll} [a]	$\phi_{C_4H_4}$	$\phi_{C_3H_2}$	$\phi_{C_3H_3}$
^{89}Y (a^2D)	69	1.00	0.24	0.02
^{89}Y (a^2D)	116	1.00	0.16	0.20
^{90}Zr (a^3F)	69	1.00	0.14	
^{93}Nb (a^6D)	71	1.00	0.04	
^{98}Mo* (a^5S)	71	1.00		

[a] E_{coll} in kJ/mol.

Nb (a^6D) + 2-Butyne. Both NbC_4H_4 and NbC_3H_2 were observed at E_{coll} = 71 kJ/mol. The lab angular distributions and TOF spectra were qualitatively similar to those obtained for Zr and are not shown. In fact, for CH_4 elimination, identical CM distributions were used to simulate the Nb and Zr data (Figure 13). Formation of $NbC_4H_4 + H_2$ was dominant, with $\phi_{NbC_3H_2}/\phi_{NbC_4H_4}$ of 0.04:1.00 (Table 1). To check for reactions of low-lying excited states in the Nb atomic beam, photodepletion studies were performed on the ground a^6D state using REMPI. Concurrent with a 24 (±4)% integrated depletion of the Nb atomic beam was a 22 (±4) and 23 (±3)% depletion of the NbC_3H_2 and NbC_4H_4 signals, respectively, demonstrating that the reactions primarily involved ground-state Nb atoms.

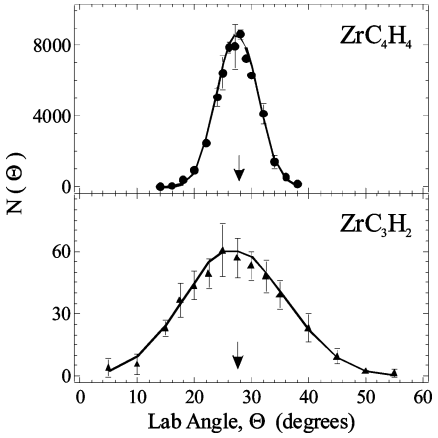

Figure 12. Lab angular distributions for ZrC_4H_4 (solid circles) and ZrC_3H_2 (solid triangles) products from the Zr + 2-butyne reactions recorded at E_{coll} = 69 kJ/mol. Distributions were normalized to the same data acquisition time. Arrows denote center of mass angle for each system.

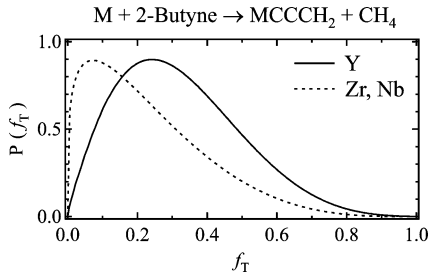

Figure 13. Translational energy release distributions for MC_3H_2 products from M + 2-butyne reactions, scaled by the estimated total available energy.

Mo (a^7S) and Mo (a^5S) + 2-Butyne.* For both ground-state Mo (a^7S) and excited-state Mo* (a^5S), only H_2 elimination was observed from reactions with 2-butyne. Simulations for H_2 elimination were qualitatively similar to those obtained for Zr and Nb.

Discussion

Nonreactive Scattering. As already noted, nonreactive scattering has been modeled as involving two processes. In physical terms, species scattered in the forward direction ($\theta \approx 0°$) resulted from collisions that did not involve complex formation. These collisions are nearly elastic, supporting the notion of minimal interaction between propyne or 2-butyne and the metal atom in these scattering events. The forward−backward symmetric contribution is a result of the decay of long-lived π-association complexes associated with the addition of the C≡C triple bond to the metal.[31]

The extent of forward scattering relative to the decay of a long-lived complex is related to the ability of the ground electronic-state metal atom reactants to form the bound M−propyne or M−butyne intermediate. The fraction of complexes decaying back to reactants also depends on the ability of these complexes to go on to reaction, leading to the elimination of a small molecule. The addition of the ethyne C≡C bond to second-row metal atoms has been investigated theoretically by Siegbahn.[33] For each system, the M−ethyne complex has a different metal electronic configuration than the separated reactants. In Figure 14, the theoretical results obtained by Siegbahn for ground-state complexes have been adapted for reactions of 2-butyne by making the reasonable assumption that the π-complexes involving M + 2-butyne are similar to those

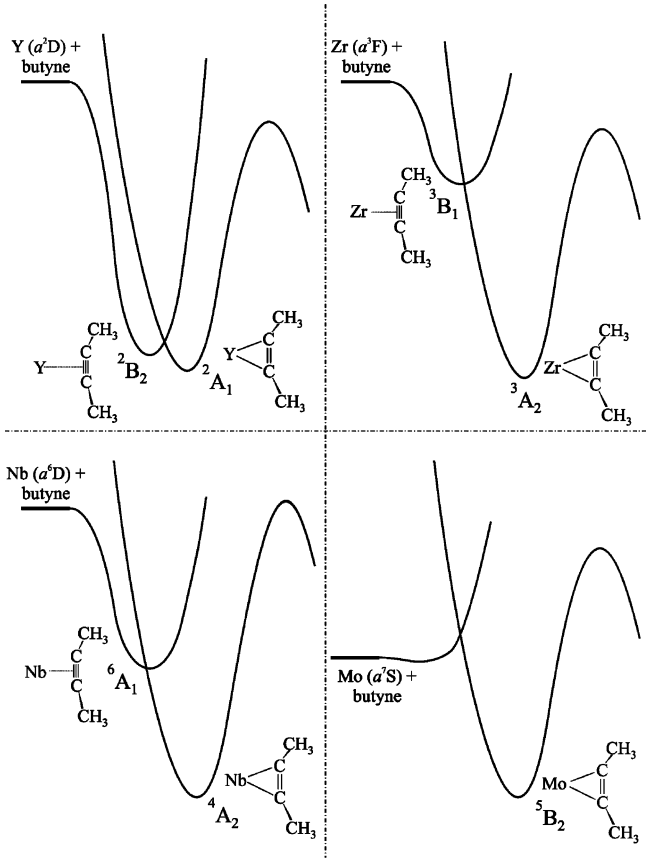

Figure 14. Schematic potential energy surfaces for M + 2-butyne entrance channel.

for M + ethyne. The curves shown in Figure 14 representing excited-state longer range metal−butyne complexes were estimated based on the following considerations: For Y (doublet, $4d5s^2$) and Zr (triplet, $4d^25s^2$), promotion of a 5s electron to a 4d (or 5p) orbital is required to form the ground-state M−alkyne complex. For Nb (sextet, $4d^4\{^5D\}5s$) and Mo (septet, $4d^5\{^6S\}$-5s), a 4d electron must undergo a spin flip to form the ground-state complex with an alkyne.[33] Theoretical calculations on reactions involving alkenes can be used to provide insight into the nature of the excited-state metal−alkyne complexes. For example, the addition of Y (a^2D) to C_2H_4 can lead to the formation of a long-range $^2B_2$ complex bound by 69 kJ/mol, or a $^2A_1$ complex bound by 93 kJ/mol.[34,35] For Y + C_2H_2, a long-range $^2B_2$ complex should be bound by approximately 170 kJ/mol.[33] For Zr (a^3F) + C_2H_4, a long-range $^3B_1$ complex was found to be bound by 40.6 kJ/mol, as compared to 118.0 kJ/mol for the ZrC_2H_4 ($^3A_2$) complex.[36] Assuming a similar situation for Zr + C_2H_2 places a long-range $^3B_1$ complex at about 170 kJ/mol below the reactants, as compared to 238 kcal/mol for ZrC_2H_4 ($^3A_2$).[33] Although calculations at the same level of theory have not been carried out for Nb, older calculations on Nb + C_2H_4 have found the long-range $^6A_1$ complex to be as strongly bound as the $^4A_2$ complex.[34] Inspection of the electronic configuration, however, suggests that for alkynes, the long-range $^6A_1$ complex will be destabilized relative to the ground state ($^4A_2$) due to a repulsive interaction between a singly occupied d orbital and the out-of-plane alkyne π-bonding orbital. Thus, the long-range $^6A_1$ alkyne complex is anticipated to lie 84−146 kJ/mol above the ground-state $^4A_2$ complex. Finally, for Mo, a septet complex with C_2H_4 was found to lie 4−8 kJ/mol below reactants.[4] For alkynes, a weakly bound septet complex will likely be destabilized by an occupied d orbital interacting with the out-of-plane π-system.

The absence of wide-angle scattering for ground-state Mo (a^7S) atoms indicates that the cross-section for complex formation, which requires intersystem crossing to the quintet surface, is very small. For Y, on the other hand, the cross-section for initial complex formation is very large due to the strongly bound nature of the long-range $^2B_2$ complex. While a fraction of these evolve to the $^2A_1$ surface and react, a substantial fraction decays back to reactants. The small percentage of symmetric nonreactive scattering for Zr is due to the weaker binding of the long-range $^3B_1$ complex and efficient crossing to the more strongly bound reactive $^3A_2$ surface where the small C−H bond-activation barrier favors decay to products. For Nb, a larger fraction of complexes decay back to reactants because intersystem crossing to the low-spin $^4A_2$ surface is necessary for the reaction to occur. For Mo* (a^5S), the bound $^5B_2$ Mo−propyne complex is readily accessed and can go directly on to form products.

C−H and C−C Insertion. Once formed, the M−propyne intermediate may decay back to reactants or undergo insertion. Three possible insertion processes are possible: (1) αC−H insertion into the sp hybridized C−H bond, (2) C−C insertion into the sp−sp^3 hybridized C−C bond, or (3) β-C−H insertion into the sp^3 hybridized C−H bonds of the methyl group. Siegbahn calculated the C−H bond insertion barriers for all second-row transition metal atoms with ethyne.[33] We present here TS energies that have been modified in accord with more recent calculations.[27] Thus, for Y, Zr, Nb, and Mo reactions with propyne, the α-C−H bond insertion barriers are −33.0, −31.8, 14.2, and 74.1 kJ/mol relative to ground-state reactants, respectively.[27] While the barriers for β-C−H insertion in these systems have not been calculated, our studies of reactions involving propene[10] and four butenes[8] have provided compelling evidence that β-C−H insertion barriers into sp^3 hybridized C−H bonds of methyl substituted alkenes are substantially lower than for α-C−H insertion. This explains as to why, for example, in previous room-temperature studies of reactions involving transition metal atoms with alkenes, propene was found to be nearly an order of magnitude more reactive than ethene.[4,34] Although the proximity of the β-H atoms may be less optimal for alkynes than for alkenes, because M−alkyne binding energies are substantally greater than in M−alkene systems,[3,4] for reactions of Y, Zr, and Nb with propyne and 2-butyne, it seems certain that the barriers for β-C−H insertion will lie well below the energy of the separated M + alkyne reactants.

To date, there have been no calculations of the potential energy barriers for C−C insertion of metal atoms in alkene and alkyne reactions. However, for reactions of saturated hydrocarbons such as ethane, barrier heights for C−C insertion are larger than C−H bond insertion barriers by 40−80 kJ/mol for neutral metal atom reactions.[3,4] Thus, C−C insertion is generally not competitive with C−H insertion, except for systems such as cyclopropane,[9,10] where C−C ring strain leads to a substantial decrease in barrier heights; in some cases (e.g., Mo), the calculated C−C insertion barriers actually lie lower than those for C−H insertion.[9,10]

In previous studies of reactions of second-row transition metal atoms with propene,[9,10] although C−C activation leading to the production of $MCH_2 + C_2H_4$ was observed, the reaction mechanism did not involve C−C insertion. Instead, the reaction was initiated by π-complex formation, followed by β-C−H insertion and H atom migration, ultimately leading to the formation of a four-membered cyclic metallocyclobutane complex that decomposes to $MCH_2 + C_2H_4$.[9,10] Reactions of propyne and 2-butyne are likely initiated by addition to the C−C triple bond, in these cases forming metallocyclopropene complexes. Although subsequent β-C−H insertion may occur, the four-membered cyclic intermediate in this case will contain a C=C bond (metallacyclobutene). Because of ring strain, the formation of such intermediates is not as thermodynamically favorable as for metallacyclobutanes. To better assess the role of H atom migration in alkyne reactions, we carried out a limited study of the reaction of Y + allene. Allene (CH_2=C=CH_2) is a structural isomer of propyne (CH_3CCH). The enthalpies of formation of both isomers are nearly identical,[37] and both reactions should be initiated by the formation of π-association complexes. At a collision energy of 84 kJ/mol, the reaction dynamics and branching ratios between $YC_2H + CH_3$ and $YC_3H_2 + H_2$ are essentially the same for propyne and allene. This strongly suggests that following the formation of the π-association complex, H atom migration is facile.

H_2 Elimination. For reactions with propyne, all metals produce $MC_3H_2 + H_2$ products. Concerted H_2 elimination from the CH_3 moiety in the initially formed π-association complex is expected to involve a large potential energy barrier and is not expected to play an important role. Thus, H_2 elimination must involve C−H insertion, H atom migration, or both. As discussed previously, for propyne, activation of the α-C−H bond (H−$CCCH_3$) is favorable for Y, Zr, and Nb. A mechanism connecting the H−M−$CCCH_3$ intermediate to H_2 elimination involves γ-H migration to form H_2MCCCH_2, which could then undergo H_2 elimination forming $MCCCH_2 + H_2$. However, as already noted, β-C−H bond insertion producing an $HCCCH_2$−M−H intermediate is also likely to be favorable. This complex may then undergo either α- or γ-H migration to form M(HC-CCH) or $MCCCH_2$ products, respectively. Despite the fact that the propargylene (HCCCH) isomer has been calculated to be 134.7 kJ/mol more stable than vinylidenecarbene ($CCCH_2$),[38] we expect the M−$CCCH_2$ binding energies to be much stronger than those for M−HCCCH,[39] resulting in similar energetics for the formation of these two isomers. In summary, it seems likely that both α- and β-C−H bond-activation mechanisms can occur and that both MC_3H_2 product isomers can be formed.

In the preceding paragraphs, two alternative sequential mechanisms for H_2 elimination were suggested. The strong similarity between the dynamics of Y reactions with propyne and allene provide strong evidence that H atom migration is indeed facile. However, theoretical calculations on a number of simple M−hydrocarbon systems have shown that H_2 elimination frequently proceeds by concerted mechanisms involving multicentered transition states (MCTS).[34,36,40,41] For M + propyne and M + 2-butyne, a larger translational energy release was observed for YC_3H_2 products than for MC_3H_2 (M = Zr, Nb, Mo, or Mo*). Similar behavior was observed for other systems[9,8,21,31] and provides strong evidence that the barrier for H_2 elimination is large in reactions with yttrium. While no calculations have been performed for M + propyne, it seems likely that there MCTS exist for concerted H_2 elimination that may in fact lie below those for sequential processes.

For reactions with 2-butyne, following formation of the π-complex, the metal atom can activate a β-C−H bond, leading to H−M−$CH_2C{\equiv}CCH_3$. A mechanism for H_2 elimination from this intermediate involves α-H migration, eventually leading to M=$CHCCCH_3$. Using $\Delta H_f(HCCCCH_3) \approx 502$ kJ/mol,[24] and assuming $D_o(M{=}CHCCCH_3) \approx D_o(M{=}CH_2)$, this channel should be ∼63 kJ/mol endoergic for Y and Mo, and roughly thermoneutral for Zr and Nb. This is not consistent with the $P(E)$ distributions required to fit the $E_{coll} \approx 69$ kJ/mol data, which all contain high-energy tails extending out to 120−160

kJ/mol (for Y, see Figure 11). Instead, formation of a metal diethyne complex, $M(C_2H_2)_2$, should be quite exoergic (≈100 kJ/mol for Y),[28] consistent with the $P(E)$ distributions in Figure 11 and observed for the other metals.

CH_3 Elimination. For reactions with propyne, methyl elimination is only observed for reactions of Y (a^2D) and then only at collision energies of 69 kJ/mol and above. A thermodynamic threshold of 63 ± 8 kJ/mol has been inferred from the data analysis. We have previously observed an analogous channel for reactions of Y (a^2D) + ethyne (elimination of H atoms), where we determined $D_o(Y-CCH) = 461.1 \pm 8.4$ kJ/mol.[21] Using this measured bond energy along with known thermodynamic values,[14] assuming that the internal energy of the propyne reactant is zero, the reaction endoergicity for $YC_2H + CH_3$ can be calculated to be 56.5 ± 8.4 kJ/mol, in good agreement with the threshold observed in this work. Our finding that the observed threshold coincides with the thermodynamic threshold suggests that CH_3 elimination occurs without any significant barrier above the reaction endoergicity.[21]

The absence of CH_3 elimination for reactions of propyne with Zr, Nb, and Mo is probably a consequence of the weak M−CCH bond strengths for these elements as compared to that for Y−CCH. Although no experimental or calculated bond energies are available for these systems, it is probable that these channels are energetically closed even at the highest collision energies studied. For Mo*, the substantial electronic energy makes CH_3 elimination energetically feasible, yet this process was not observed. There are two mechanistic pathways to CH_3 elimination in the Y + propyne and 2-butyne reactions. The first step is the formation of the Y-alkyne complex. Simple C−C bond cleavage can then occur with a loss of CH_3 directly via a barrierless dissociation. Alternatively, insertion into an $sp-sp^3$ C−C bond forming a $R-C\equiv C-Y-CH_3$ intermediate may occur, followed by CH_3 loss. Because both pathways correspond to barrierless elimination of CH_3, our data cannot be used to discriminate between the two possible mechanisms for CH_3 elimination.

For Y + propyne and 2-butyne, as the collision energy was increased, a striking rise in the amount of CH_3 elimination was observed. From previous studies of Y reactions, elimination of H_2 is expected to proceed via a tight TS (i.e., over a potential energy barrier);[1−17] a similar situation is expected for CH_4 elimination in the case of 2-butyne. Elimination of a radical such as CH_3, however, should proceed via a loose TS (i.e., no potential energy barrier above the product asymptote). In a statistical model, the loose TS for CH_3 elimination leads to an increased number of open states as compared to the tight TS for H_2 and CH_4 elimination. Thus, as the collision energy is increased, the reaction rate increases more rapidly for the elimination of CH_3 than for the elimination of H_2 or CH_4, allowing CH_3 elimination to become more competitive at higher collision energies.

CH_4 Elimination. The reaction M + 2-butyne → $MC_3H_2 + CH_4$ presents a highly exoergic product channel involving C−C bond cleavage. As far as we know, this is the first observation of methane elimination in neutral transition metal−hydrocarbon reactions. For Y, this channel lies approximately 140 kJ/mol below the separated reactants, which is about 40 kJ/mol lower than the products from H_2 elimination.

It is clear that H atom migration must occur for this channel to be operative. As already noted, formal C−C insertion is not necessarily a prerequisite for C−C bond fission. One interesting aspect of the M + propyne and M + 2-butyne reactions is that they allow a comparison of H_2 elimination and CH_4 elimination,

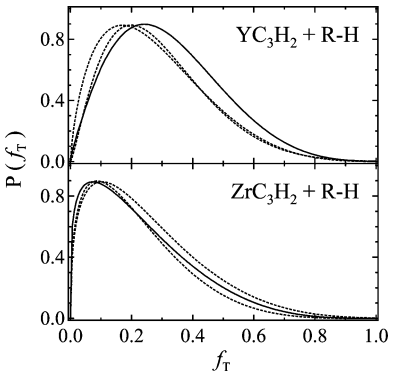

Figure 15. Scaled translational energy release distributions for H_2 (dashed lines) and CH_4 (solid lines) elimination from M + propyne and 2-butyne reactions, respectively.

respectively, accompanied by the formation of the same product, MC_3H_2. In Figure 15, we present scaled translational energy release distributions, $P(f_T)$, for H_2 elimination (dashed lines) and CH_4 elimination (solid lines) for YC_3H_2 and ZrC_3H_2 formed from the reaction with propyne and 2-butyne, respectively.[42] For both metals, two distributions are included for H_2 elimination at different total energies that bracket the total energy for CH_4 elimination (e.g., $E_{tot} = 138$ and 188 kJ/mol for $ZrC_3H_2 + H_2$ and $E_{tot} = 176$ kJ/mol for $ZrC_3H_2 + CH_4$). The distributions for Zr are notably similar, with both H_2 and CH_4 elimination $P(f_T)$s peaking near $\langle f_T \rangle = 0.1$. The small $\langle f_T \rangle$ values for these distributions are consistent with the absence of a significant potential energy barrier in the exit channel (other than centrifugal barriers). Similar $P(f_T)$ values have been observed experimentally for $Zr + C_2H_4$.[31] For Y, the $P(E)$ values for the elimination of H_2 and CH_4 show that a greater fraction of the available energy was partitioned into translational energy than for the Zr reactions, suggesting a potential energy barrier in the exit channel for both H_2 and CH_4 elimination in the Y reaction.[9,18,21,43]

As shown in Figure 15, the $P(f_T)$ distribution for CH_4 elimination from Y + 2-butyne peaks further away from the zero of translational energy than those for H_2 elimination from Y + propyne. Thus, a larger amount of translational energy is observed in the system with more product vibrational degrees of freedom. This indicates that for the formation of a given unsaturated metal species involving Y, the exit channel barrier for CH_4 elimination is larger than that for H_{-2} elimination. This is consistent with expectations for the microscopic reverse process (i.e., that insertion into C−H bonds involves barriers larger than for insertion into H_2).[3,4,44] Such behavior may be easily understood by considering the directionality of the participating bonds. In the case of H_2, the spherical s orbitals can participate in multicentered bonding, thereby stabilizing the transition state. For CH_4, on the other hand, the highly directional sp^3 hybridized C−H bond is nearly broken near the top of the barrier.

C−C versus C−H Activation. For propyne reactions, competition between C−C and C−H bond activation was only seen for yttrium. The observed product branching ratio, $\phi_{YC_2H}/\phi_{YC_3H_2}$, was 0.11:1.00 at $E_{coll} = 99$ kJ/mol and decreased at lower collision energies. For M + 2-butyne, the competition between C−H and C−C bond activation can be understood by comparing the product branching ratios (Table 1). For Y, C−C bond activation (as both CH_3 and CH_4 elimination) constituted as much as 27% of the total products at $E_{coll} = 116$ kJ/mol. Elimination of CH_4 was also significant for Zr, albeit less so than for Y. The $NbC_3H_2 + CH_4$ channel was observed at E_{coll}

= 71 kJ/mol but only constituted 4% of the total product signal. No CH_4 or CH_3 elimination was observed for Mo* (a^5S_2), despite the fact that these channels are thermodynamically open. This absence of C−C activation is quite intriguing, particularly in light of the fact that Mo* (a^5S_2) activates the C−C bonds of cyclopropane more effectively than C−H bonds. While this behavior for butyne clearly requires further investigation, the lack of C−C bond activation for Mo* (a^5S_2) + butyne may simply be because the H_2 elimination channel is very efficient. In summary, as the second transition metal row is traversed, C−C bond-activation products become less competitive relative to C−H bond-activation products for reactions with 2-butyne.

As mentioned earlier, a comparison of C−H insertion barriers for alkanes, alkenes, and alkynes indicates that C−H insertion barriers decrease with increasing strength of the C−H bond being activated. We have now completed studies of the reactions of yttrium with the series propane, propene, and propyne, and so some comments can be made as to whether a similar trend exists for C−C activation barriers. In reactions of Y with propane, no products corresponding to C−C activation were observed, even at high collision energies. For Y + propene, C−C activation products were observed ($YCH_2 + C_2H_4$), with a branching ratio $\phi_{YCH_2}/\phi_{YC_3H_4} = 0.48{:}1.00$ at $E_{coll} = 105$ kJ/mol.[10] In the current study, for Y + propyne at $E_{coll} = 99$ kJ/mol, the branching ratio $\phi_{YC_2H}/\phi_{YC_3H_2} = 0.11{:}1.00$. It is thus notable that C−C activation of propene and propyne has only been observed in reactions with yttrium. Apparently, yttrium is unique among the metal atoms studied. One major factor that contributes to this rich chemistry of Y is the presence of a potential energy barrier in the exit channel for the most thermodynamically favored channel, the elimination of H_2. This allows less thermodynamically favorable products to be competitive. For butyne reactions, this factor likely also plays an important role in facilitating competition with dynamically less favorable channels.

Conclusion

The collisions of early second-row transition metal atoms with propyne and 2-butyne were studied using crossed molecular beams. The reaction M + propyne → $MC_3H_2 + H_2$ was observed for all metal atoms at $E_{coll} = 54$ kJ/mol. On average, a larger fraction of the total available energy was released as translational energy for Y ($f_T = 0.29$) as compared to Zr and Nb ($f_T = 0.25$). Our finding that the reaction dynamics for Y + propene and allene, two structural isomers having nearly identical enthalpies of formation, is similar provides strong evidence that H atom migration is facile. The observation of MoC_3H_2 for Mo (a^7S) demonstrated the ability of the septet reactants to access the quintet reaction coordinate, in contrast to the situation observed for Mo (a^7S) + ethane.[17]

An energetic threshold of 63 ± 8 kJ/mol was determined for the C−C fission reaction Y + propyne → $YC_2H + CH_3$, in agreement with our previous measurement for $D_o(Y{-}CCH)$.[21] For reactions with 2-butyne, elimination of H_2 was observed for all four metal atoms, while CH_4 elimination was observed for Y, Zr, and Nb. Elimination of CH_3 was only observed for Y. Product branching ratios indicated that as the second transition metal row was traversed, products arising from C−C bond activation became less competitive relative to those from C−H bond activation.

The formation of $MC_3H_2 + CH_4$ in the M + 2-butyne reaction facilitated a comparison of exit channel dynamics to the $MC_3H_2 + H_2$ product channel from M + propyne reactions. The translational energy release distributions, $P(f_T)$, for ZrC_3H_2 and NbC_3H_2 were similar in shape for these two reactions, consistent with both H_2 and CH_4 elimination involving a loose transition state. For Y, considerably more translational energy was released than for Zr or Nb, suggesting a potential energy barrier in the exit channels.

Acknowledgment. This work was funded by the National Science Foundation. R.Z.H. thanks the Department of Education for a fellowship, and J.J.S. thanks the Cornell Graduate School, the Department of Education, and the Franz Roessler Foundation for fellowships. The authors thank Yumiko Nakatsuka for carrying out the experiments on Y + allene.

References and Notes

(1) Crabtree, R. H. *Chem. Rev.* **1995**, *95*, 987.
(2) Shilov, A. E.; Shul'pin, G. B. *Chem. Rev.* **1997**, *97*, 2879.
(3) Siegbahn, P. E. M.; Blomberg, M. R. A. Oxidative Addition Reactions. In *Theoretical Aspects of Homogeneous Catalysis*; van Leeuwen, P. W. N. M., Morokuma, K., van Lenthe, J. H., Eds.; Kluwer: Dordrecht, The Netherlands, 1995; pp 15−63.
(4) Carroll, J. J.; Haug, K. L.; Weisshaar, J. C.; Blomberg, M. R. A.; Siegbahn, P. E. M.; Svensson, M. *J. Phys. Chem.* **1995**, *99*, 13955.
(5) Rybtchinski B.; Milstein, D. *Angew. Chem., Int. Ed.* **1999**, *38*, 870.
(6) Armentrout, P. B. *Annu. Rev. Phys. Chem.* **1990**, *41*, 313.
(7) Weisshaar, J. C. *Acc. Chem. Res.* **1993**, *26*, 213.
(8) Schroden, J. J.; Wang, C. C.; Davis, H. F. *J. Phys. Chem. A* **2003**, *107*, 9295.
(9) Hinrichs, R. Z.; Schroden, J. J.; Davis, H. F. *J. Am. Chem. Soc.* **2003**, *125*, 861.
(10) Hinrichs, R. Z.; Schroden, J. J.; Davis, H. F. *J. Phys. Chem. A* **2003**, *107*, 9284.
(11) Niu, S.; Hall, M. B. *Chem. Rev.* **2000**, *100*, 353.
(12) Wittborn, C. A. M.; Costas, M.; Blomberg, M. R. A.; Siegbahn, P. E. M. *J. Chem. Phys.* **1997**, *107*, 4318.
(13) Moore, C. E. *Atomic Energy Levels*; National Bureau of Standards: Washington, DC, 1971.
(14) Berkowitz, J.; Ellison, B.; Gutman, D. *J. Phys. Chem.* **1994**, *98*, 2744.
(15) Jones, W. D.; Feher, F. *J. Acc. Chem. Res.* **1989**, *22*, 91.
(16) (a) Stoutland, P. O.; Bergman, R. G. *J. Am. Chem. Soc.* **1985**, *107*, 4581. (b) Ibid, *J. Am. Chem. Soc.* **1988**, *110*, 5732.
(17) Hinrichs, R. Z.; Willis, P. A.; Stauffer, H. U.; Schroden, J. J.; Davis, H. F. *J. Chem. Phys.* **2000**, *112*, 4634.
(18) Stauffer, H. U.; Hinrichs, R. Z.; Schroden, J. J.; Davis, H. F. *J. Phys. Chem. A* **2000**, *104*, 1107.
(19) Schroden, J. J. and Davis, H. F., unpublished results.
(20) Porembski, M.; Weisshaar, J. C. *J. Phys. Chem. A* **2000**, *104*, 1524.
(21) Stauffer, H. U.; Hinrichs, R. Z.; Willis, P. A.; Davis, H. F. *J. Chem. Phys.* **1999**, *111*, 4101.
(22) These values are estimated using the measured value for $D_o(Y{-}C_2H)$ (ref 21) and tabulated $\Delta H°_f$ values for hydrocarbon radical fragments (refs 24 and 26). We assumed $D_o(M{=}CCCH_2) = D_o(M{=}CH_2)$ (ref 25), $D_o(M{-}CCCH_3) = D_o(M{-}CCH)$ (ref 21), and $D_o(M{-}C_4H_4) = D(M{=}CH_2)$.
(23) Because of the weaker bonding in the products, the values for ΔE for reactions with Nb and Zr are expected to be 40−80 kJ/mol greater than those for Y.
(24) Mebel, A. M.; Kaiser, R. I.; Lee, Y. T. *J. Am. Chem. Soc.* **2000**, *122*, 1776.
(25) Siegbahn, P. E. M. *Chem. Phys. Lett.* **1993**, *201*, 15.
(26) Thermodynamics Research Center, NIST Boulder Laboratories, M. Frenkel director. Thermodynamics Source Database. In *NIST Chemistry WebBook, NIST Standard Reference Database Number 69*; Linstrom, P. J., Mallard, W. G., Eds.; National Institute of Standards and Technology: Gaithersburg, MD, July 2001; p 20899; http://webbook.nist.gov.
(27) Energies for M + ethene included for comparison in ref 33 were subsequently revisited using the more accurate PCI-80 method (see refs 3 and 12). We adjusted the thermodynamic values for M + alkynes assuming similar changes in calculated energies to those for M + ethene.
(28) For $M(C_2H_2)_2$, the binding energy of the second C_2H_2 unit to M was assumed to be the same as that of the first C_2H_2 unit.
(29) Willis, P. A.; Stauffer, H. U.; Hinrichs, R. Z.; Davis, H. F. *Rev. Sci. Instrum.* **1999**, *70*, 2606.
(30) Powers, D. E.; Hansen, S. G.; Geusic, M. E.; Puiu, A. C.; Hopkins, J. B.; Dietz, T. G.; Duncan, M. A.; Langridge-Smith, P. R. R.; Smalley, R. E. *J. Phys. Chem.* **1982**, *86*, 2556.
(31) Willis, P. A.; Stauffer, H. U.; Hinrichs, R. Z.; Davis, H. F. *J. Phys. Chem. A* **1999**, *103*, 3706.
(32) Proch, D.; Trickl, T. *Rev. Sci. Instrum.* **1989**, *60*, 713.
(33) Siegbahn, P. E. M. *Theor. Chim. Acta* **1994**, *87*, 277.

(34) Porembski, M.; Weisshaar, J. C. *J. Phys. Chem. A* **2001**, *105*, 6655.
(35) Blomberg, M. R. A.; Siegbahn, P. E. M.; Svensson, M. *J. Phys. Chem.* **1992**, *96*, 9794.
(36) Porembski, M.; Weisshaar, J. C. *J. Phys. Chem. A* **2001**, *105*, 4851.
(37) Yu, H.-G.; Muckerman, T. J. *J. Phys. Chem. A* **2005**, *109*, 1890.
(38) Kaiser, R. I.; Ochsenfeld, C.; Head-Gordon, M.; Lee, Y. T.; Suits, A. G. *J. Chem. Phys.* **1997**, *106*, 1729.
(39) Glendening, E. D.; Strange, M. L. *J. Phys. Chem. A* **2002**, *106*, 7338.
(40) Bayse, C. A. *J. Phys. Chem. A* **2002**, *106*, 4226.
(41) Glendening, E. D. *J. Phys. Chem. A* **2004**, *108*, 10165.
(42) CM distributions for Zr and Nb were very similar for these reactions; thus, similar considerations as those discussed for Zr would be expected to hold for Nb as well.
(43) Schroden, J. J.; Teo, M.; Davis, H. F. *J. Phys. Chem. A* **2002**, *106*, 11695.
(44) Low, J. J.; Goddard, W. A., III. *J. Am. Chem. Soc.* **1984**, *106*, 8321.